Science and Technology of Welding & Joining,

Volume 15, Number 6, August 2010, pp. 479-485

Energy and force analysis of linear friction welds in a medium carbon steel

Usani U. Ofem[1], Paul A. Colegrove[1], Adrian Addison[2] and Michael J. Russell[2].

[1]Cranfield University, Cranfield, Bedfordshire MK43 0AL, United Kingdom.
[2]TWI Ltd., Granta Park,Great Abington, Cambridge, CB21 6AL, United Kingdom.

Abstract

The linear friction welding process is rapidly developing into an important manufacturing technology for high quality joining of engineering materials. The energy required for Linear Friction Welding is an important issue due to economic and environmental reasons, but is not currently fully understood. This paper describes a comprehensive evaluation of the energy input during Linear Friction Welding of a medium carbon steel with different process parameters. This calculation is based on an analysis of force and displacement data from the machine, which takes momentum into account. The analysis shows that energy input to the weld is minimised with high frequencies and rubbing velocities, however there is a considerable amount of energy lost in oscillating the machine tooling under these conditions. Furthermore, analysis of the force indicates that a peak load occurs just prior to the samples being aligned which is probably caused by ploughing of the samples during welding.

1 Introduction

Linear friction welding (LFW) has many advantages over conventional welding processes. It is robust, repeatable, fast, and is capable of producing high quality joints in many engineering metals and metal combinations. Despite these benefits, the number of industrial applications is limited and confined to the aerospace industry. Hence the number of published articles on this topic is relatively small, and those available focus on describing the process[1-3], modelling [2,4-6], microstructure and characterisation[7,8] and residual stress measurement [9-11]. Due to the process being applied primarily to titanium alloys, most articles relate to the welding of this material, although there are exceptions[7].

The LFW process works by holding one component stationary and oscillating another component against it under an applied load[1,3,9]. This is shown in the schematic diagram of the equipment used for the process in Fig. 1(a). The motion between the parts generates heat which causes the material at the interface to plasticise and soften. As the process progresses, the applied load causes extrusion of the material from the joint, and any surface impurities are removed in the flash. One of the advantages of this process is that the parts can be of arbitrary shape, unlike the related process of rotary friction welding where the parts must be cylindrical.

Much of the early reported work on the process was performed by Vairis and Frost[1,2,4], and describes how the process may be divided into four phases:

- Phase I – Initial phase. During this phase heat is produced by columbic friction between the rubbing surfaces. Asperity contact exists between the two surfaces, and as heat is generated, the asperities soften and deform, increasing the true area of contact between the parts.
- Phase II – Transition phase. During this phase the true area of contact increases to 100% of the cross-sectional area. This transition is accompanied by an increase in the force required to oscillate the parts.
- Phase III – Equilibrium phase. During this phase the shear force reaches a steady state value and significant axial shortening occurs through the generation of flash. The plastic zone gets progressively larger during this phase.
- Phase IV – Deceleration phase. The relative motion is ceased and the two parts are aligned. In some applications an additional forging force may also be applied.

Addison[3] classifies these phases slightly differently and divides them into conditioning (phase I), friction (phases II and III) and forge (phase IV).

Although attempts have been made to predict the energy input from either simple formulas or from model predictions[1,2,4,5,8], no authors have yet demonstrated how it may be calculated from the force and displacement measurements from the machine. The energy input is crucial to whether successful welding conditions are achieved[1,4]. In addition, the energy usage of the process is of interest due to both economic and environmental reasons. Therefore the objectives of this study were:

- Perform a systematic set of experiments at different frequencies and rubbing velocities to determine how these parameters affect the heat generation and whether successful welds are produced.
- Use this data to determine the most efficient approach for LFW in this case.

2 Methodology

2.1 Experimental

The experiments used a hydraulically operated LFW machine at TWI, Cambridge. Fig. 1(a) is a schematic diagram which explains how it works. The core of the machine is a 200kN hydraulic servo actuator situated on top of the machine which is connected to an oscillating carriage suspended within hydrostatic bearings. The stationary tooling is connected to a second hydraulic cylinder which is used to apply the friction pressure to the sample. The material used for the experiments was BS 970-3:1991 80M40 steel, with dimensions 63.5mm x 12.7mm x 75±1mm. Hydraulically operated clamps were used to hold the samples in position. There are a number of devices on the machine for process monitoring which include:

- Oscillator position, x by linear variable displacement transducer;
- Oscillation in-plane load, F_l by a load cell between the servo actuator and oscillating tooling;
- Axial position, y by LVDT on the machine table;
- Axial load, F_a by load cell between the actuator and machine table and pressure transducer in the hydraulic system.

A constant friction pressure of 125 MPa corresponding to a force of 100.8 kN for the 12.7×63.5 mm specimens was applied to all of the welding samples. A constant burn-off distance of 3.5 mm was used for all the specimens. In the experimental programme, the oscillation frequency and amplitude were varied, to give peak rubbing velocities of 470, 549, 710 and 863 mm s^{-1}. These correspond to average rubbing velocities of 300, 350, 450 and 550 mm s^{-1}. The maximum rubbing velocity was determined by assuming sinusoidal motion of the oscillating workpiece, so the displacement, x can be approximated by[12]:

$$x = A\sin(\omega t + \delta) \tag{1}$$

Where A is amplitude of oscillation, ω is angular velocity and equals $2\pi f$, f being the frequency of oscillation and δ is the phase shift. This equation is differentiated with respect to time to determine the velocity, v.

$$v = \frac{dx}{dt} = A\omega\cos(\omega t + \delta) \tag{2}$$

Hence, the maximum velocity may be given by:

$$v_{\max} = A2\pi f \tag{3}$$

Fig. 2 shows the parameters that were used to achieve the four rubbing velocities. Four welds were made at each condition to investigate the consistency of the process.

2.2 Analysis of Energy Input

The energy going into each weld can be determined from the load cell and displacement measurements made by the machine. However, as shown in the schematic diagram in Fig. 1(a) the load is not being measured at the sample, but rather between the tooling and the servo actuator. The energy going into the sample requires the force at the sample interface, F_{int} to be determined, which is shown in Fig. 1(b).

The instantaneous power, $\dot{q}$ going into the sample is given by:

$$\dot{q} = F_{\text{int}} v \tag{4}$$

To calculate the total energy, E_x to make the weld, the instantaneous power is integrated over the weld duration:

$$E_x = \int_0^T \dot{q} dt = \int_0^T F_{\text{int}} v dt \tag{5}$$

To calculate the force at the interface, a free body analysis of the oscillating tooling in Fig. 1(b) gives:

$$F_{\text{int}} = F_l - Ma \tag{6}$$

The positive force convention is shown on Fig. 1(b). Note that while F_l is positive downwards, F_{int} is positive upwards. In addition, the mass M of the oscillating system equals 224 kg. This value is compared with the energy that goes into the oscillating system:

$$E_0 = \int_0^T F_l v dt \tag{7}$$

The preceding analysis requires estimates of both the velocity and the acceleration. This can be achieved numerically in a straightforward manner, once the position at different discrete values in time is known. Hence, for the velocity a simple two-point, central finite difference approximation is used for the first order derivative[13], i.e:

$$v_1 = \frac{1}{2h}\left(-x_0 + x_2\right) \tag{8}$$

Where v_1 is the velocity at a point in time (the "present time level" denoted 1), x_0 and x_2 are the positions at the previous and future time levels and h is the time step size. Similarly the acceleration can be found from a three-point central finite difference for the second order derivative:

$$a_1 = \left(\frac{x_2 - 2x_1 + x_0}{h^2} \right) \tag{9}$$

Where x_1 is the position at the present time level. Alternatively, if the displacement is sinusoidal the acceleration can be determined from the second derivative of the displacement in equation (1):

$$a = -A\omega^2 \sin\left(\omega t + \delta\right) = -\omega^2 x = -\left(2\pi f\right)^2 x \tag{10}$$

The preceding analysis has assumed:

- Friction from the hydrostatic bearings supporting the tooling is negligible.
- Movement of the samples in the tooling is minimal.
- The energy going into the specimen from the burn-off can be ignored.

3 Results and Discussion

3.1 Conditions that Gave Good Welds

Fig. 2 shows the conditions that were attempted and highlights those conditions that did not produce successful welds. In some cases the cause of the unsatisfactory weld was unsuitable welding conditions for the material being welded, and in other cases the machine struggled to produce welds at the parameters selected. Both cases involved high frequency settings.

Visual inspection of all the successfully welded test samples showed uniform and sound welded joints. The flash distribution was symmetric and even on both sides of the joint with the larger length being in the direction of oscillation. The flash was joined around the corners of all of the successfully welded samples. It was also observed that the thickness of extruded flash

was not uniform but took the shape of ridges. These observations have also been made by Vairis and Frost[1,2].

3.2 General Curves of Force, Displacement and Burn-Off

A typical plot of the machine data from one of the linear friction welds is shown in Fig. 3. This particular weld used a frequency of 30 Hz and a peak rubbing velocity of 549 mm s^{-1}. The burn-off (Fig. 3(a)), which indicates the displacement of the tooling, starts from a negative value initially. Once the two samples touch (at about 1.0 second) the value remains relatively constant before increasing toward the final value of 3.5 mm near the end of the weld. From this curve five phases of the LFW are identified: phase 0 before the samples touch and the machine is free-running; phase I the initial or conditioning phase; phase II the transition phase; phase III the equilibrium phase; and phase IV the forge phase. About 1.7 seconds is required to make this particular weld and about one second has elapsed during the free-running phase.

The axial load which is measured by the load cell and pressure transducer (Fig. 3(a)), increase to 101 kN after a short period of oscillation. The plot of the in-plane force (Fig. 3(b)) shows a rapid increase after the samples touch and then remains relatively constant thereafter. The initial increase corresponds to the increase in axial load. This contrasts with Vairis and Frost[1] who observed an increase in the in-plane force around the start of phase II. Possible reasons for the difference in the two results are:

- Vairis and Frost welded titanium whereas the current work uses steel.
- Much higher rubbing velocities and friction pressures are used in the current work which will lead to a greater power input.

In addition, the machine used by Vairis and Frost started oscillation with the samples touching so there was no phase 0. Finally, while the welds in Vairis and Frost took between 8 and 60 seconds, the welds in the current study took a maximum of 2.2 seconds.

3.3 Calculating Acceleration

The velocity and acceleration data calculated by the numerical techniques described in section 2.2, are shown in Fig. 4. Note that the acceleration estimate based on the displacement, x (Equation (10)) uses the actual displacement rather than an idealised one based on the sin function. There is considerable noise in the estimate of acceleration which uses numerical differentiation (Equation (9)) which is absent from the estimate based on the displacement (Equation (10)). For high frequency oscillations, the time spent for one cycle is reduced and as the sampling rate is kept constant at 1 ms, the resolution of the cycle in terms of measuring points will be coarsened accordingly. Nevertheless, the estimate based on the displacement (Equation (10)) is considered sufficiently accurate to be used for estimates of the energy input.

3.4 Relationship between in-plane force and interface force

Plots of the interface and in-plane force for two different welding conditions are shown in Fig. 5. See Fig. 1(b) for the sign conventions for the forces. The velocity has been inverted for clarity. To aid understanding of these plots three phases of the cycle are identified: phase *a*, the acceleration phase; phase *b*, constant velocity phase; and phase *c*, the deceleration phase. These phases are shown pictorially in Fig. 6. During the acceleration phase, *a* the interface force is generally lower than the in-plane force. This is because the force at the interface and the momentum of the tooling are additive (see equation (6)). In the constant velocity phase, *b* the interface and in-plane forces are approximately equal because the acceleration is approximately zero. During the deceleration phase, *c* the momentum subtracts from the force

at the interface so the interface force is higher than the in-plane force measured at the load cell. The difference is greatest where the velocity is near zero (i.e. at the ends of the stroke) because this is the point where the acceleration is greatest. Since the magnitude of the acceleration calculated from the displacement is proportional to the displacement multiplied by the square of the angular frequency (Equation (10)), higher oscillation frequencies increase the difference between the interface and in-plane forces.

One of the issues with the analysis is the accuracy of the estimate of acceleration. One way of validating the estimate of the acceleration is to examine the direction of the interface force. The interface force must oppose the direction of motion. i.e. friction always operates opposite to the direction of travel. The two force traces indicate that this is not always the case, particularly for the lower speed plot in Fig. 5(a). The error may be due to an error in either the load cell or displacement readings. e.g. there could be a slight delay in the readings obtained from the load cell. Another potential source of error is deflection of the samples, and finally it may also be caused by the method used to estimate the acceleration.

The interface force is approximately proportional to the velocity, particularly for the lower speed plot in Fig. 5(a). If the interface force were purely columbic then the interface force would be entirely dependent on the friction at the interface and the load applied. This is clearly not the case and it is suggested that one or more of the following factors may cause the variation in force observed:

- Rubbing velocity. Under high temperatures and pressures a sticking condition often exists between the two rubbing surfaces[14,15]. Therefore the rubbing causes shearing of the material and the flow-stress is dependant on the strain-rate of the material. Hence higher velocities increase the strain-rate leading to a greater flow stress which requires a higher interfacial force to cause the deformation.
- Interfacial area. The interfacial area between the two parts varies linearly with the displacement. Hence the maximum area is obtained when the two parts are aligned and is minimum at the maximum amplitude or displacement. This effect will lead to higher values of the interface force when the parts are aligned.
- Ploughing effects. This effect is explained in the diagrams shown in Fig. 7. This characteristic is observed in both force traces, but particularly Fig. 5(b). This ploughing effect would also explain why the flash is produced in pulses rather than being a continuous flow which has been observed by several authors[1,2,8]. It may also help to explain the ripple in the burn-off curve observed in Fig. 3(a).

Finally it was interesting to note that the peak interface force was approximately 100 kN irrespective of the welding condition. This suggests that the rubbing velocity and the associated strain-rate effects may not significantly affect the force at the interface, with interfacial area and ploughing having the dominant effect.

3.5 Energy efficiency

To analyse the energy input to the weld a series of six plots have been produced which are shown in Fig. 8. Fig. 8(a) shows a plot of the interface and in-plane energies for phases 1, 2 and 3 (the free running phase 0 is excluded). The interface energy exceeds the in-plane energy for the low rubbing velocity welds which is obviously an error in the calculation and is likely to be due to the errors in calculating the interface force which are described above. In any case, the magnitude of the error is small and it is possible to conclude that for low rubbing

velocity conditions the losses caused by oscillating the tooling and sample are negligible. However this is not the case for the high rubbing velocity welds where the energy efficiency during the welding phase can be reduced to approximately 85%.

Despite this lower efficiency at the higher frequencies the overall energy input to the weld was much lower. The main cause of this was the much shorter weld duration needed when using high rubbing velocities (Fig. 8(b)). The shorter welding time is achieved because the power input (Fig. 8(c)) is greater at the high rubbing velocities.

The plot of the overall energy consumption Fig. 8(d) which includes the energy consumed in phase 0 indicated very little difference over the range of parameters examined, although a rubbing velocity of 710 mm s^{-1} minimised the energy consumption for these particular welds. The energy consumed during phase 0 for the high rubbing velocity welds is considerably higher (13 kJ compared to 1.5 kJ) due to the energy required to oscillate the tooling at this speed. Reducing energy consumption during the free running phase by shortening its duration is one way to significantly reduce the overall energy consumption for the high rubbing velocity welds. If this were done the total energy consumption for these welds would be significantly lower than the other welding conditions. Note that the free running time in this research programme was random and this factor would be accurately controlled in a production scenario. The high energy losses to oscillate the tooling at high rubbing velocities are reflected in the overall efficiency Fig. 8(e), which includes the energy input during the free running phase 0 (unlike Fig. 8(a)).

The total weld or rubbing distance Fig. 8(f) shows little variation across the range of parameters examined. This suggests that there is a very strong relationship between the rubbing distance and the burn-off. The slightly lower values obtained for the high rubbing velocity welds are likely to be due to the higher power input for these welds which reduces the time taken to make the weld.

4 Conclusions

The main conclusions from this work are:

- Five phases were identified during the LFW process. The in-plane force had a slightly different characteristic to that observed by Vairis and Frost[1]. The difference may be due to the different parameters used in this work as well as the different materials used.
- A method for calculating the force at the weld interface from the forces measured at a load cell attached to the tooling has been demonstrated. This enabled calculation of the energy input to make the weld under different combinations of frequency and rubbing velocity.
- The energy input required to make a weld can be minimised by optimising the rubbing velocity.
- High frequency LFW is inherently less efficient, but welds can be made more quickly so overall energy usage may be reduced.
- Examining plots of the interface force and rubbing velocity versus time for different welding parameters proved particularly interesting. This showed that the peak in the force occurs just prior to the centre position and is likely to be caused by ploughing effects.

5 Acknowledgements

The authors wish to thank the Petroleum Technology Development Fund (PTDF) of Nigeria and TWI for helping to fund this work.

6 References

1. A. Vairis and M. Frost: 'High frequency linear friction welding of a titanium alloy', *Wear,* 1998, **217**, 117-131.
2. A. Vairis and M. Frost: 'On the extrusion stage of linear friction welding of Ti 6a1 4V', *Materials Science and Engineering A,* 1999, **271**, 477-484.
3. A. C. Addison: 'Linear Friction Welding of Engineering Metals', Report TWI Industrial Member Report 894/2008, TWI Ltd, Cambridge, UK, 2008.
4. A. Vairis and M. Frost: 'Modelling the linear friction welding of titanium blocks', *Materials Science and Engineering A,* 2000, **292**, 8-17.
5. W. Y. Li, T. Ma and J. Li: 'Numerical simulation of linear friction welding of titanium alloy: Effects of processing parameters', *Materials and Design*, 2009, .
6. J. Tao, T. Zhang, P. Liu, J. Li and Y. Mang: Proc. Materials Science Forum, 811-815.
7. T. Ma, W. Y. Li, Q. Xu, Y. Zhang, J. Li, S. Yang and H. Liao: 'Microstructure evolution and mechanical properties of linear friction welded 45 steel joint', *Advanced Engineering Materials,* 2007, **9**, 703-707.
8. P. Wanjara and M. Jahazi: 'Linear friction welding of Ti-6Al-4V: Processing, microstructure, and mechanical-property inter-relationships', *Metall Mat Trans A Phys Metall Mat Sci,* 2005, **36**, 2149-2164.
9. P. Frankel, M. Preuss, A. Steuwer, P. J. Withers and S. Bray: 'Comparison of residual stresses in Ti-6Al-4V and Ti-6Al-2Sn-4Zr-2Mo linear friction welds', *Materials Science and Technology,* 2009, **25**, 640-650.
10. J. Romero, M. M. Attallah, M. Preuss, M. Karadge and S. E. Bray: 'Effect of the forging pressure on the microstructure and residual stress development in Ti-6Al-4V linear friction welds', *Acta Materialia*, 2009, **57**, 5582-5592.
11. M. R. Daymond and N. W. Bonner: 'Measurement of strain in a titanium linear friction weld by neutron diffraction', *Physica B: Condensed Matter,* 2003, **325**, 130-137.
12. I. Cochin and H. J. Plass: 'Analysis and Design of Dynamic Systems', 1990, New York, Harpercollins College Div.
13. E. Kreyszig: 'Advanced Engineering Mathematics', 6th edn, 985-6; 1988, New York, John Wiley and Sons, New York,.
14. M. Maalekian: 'Friction welding - Critical assessment of literature', *Science and Technology of Welding and Joining,* 2007, **12**, 738-759.
15. A. Vairis and N. Christakis: 'The development of a continuum framework for friction welding processes with the aid of micro-mechanical parameterisations', *International Journal of Modelling, Identification and Control,* 2007, **2**, 347-355.

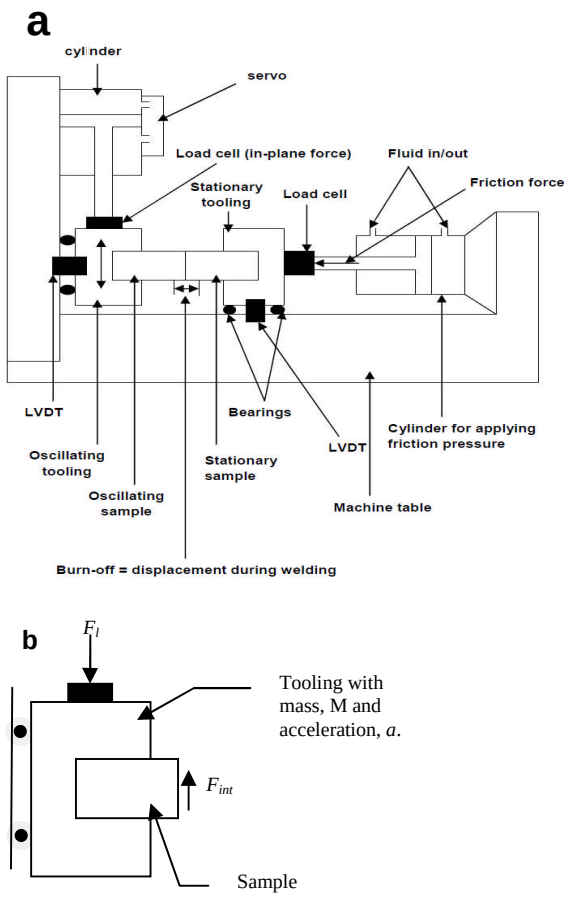

Fig. 1 Schematic diagram showing (a) how the LFW machine works, and (b) an enlarged view of the oscillating tooling.

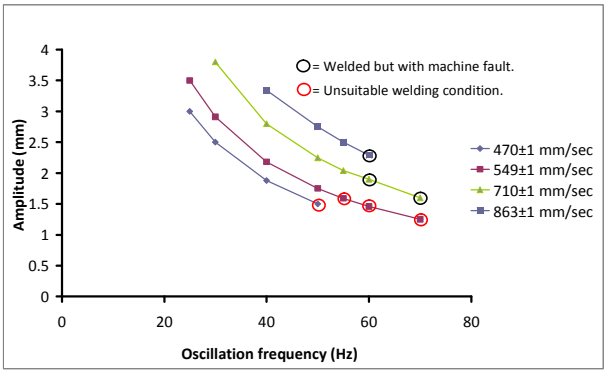

Fig. 2 Combinations of oscillating frequency and amplitude for different maximum rubbing velocities.

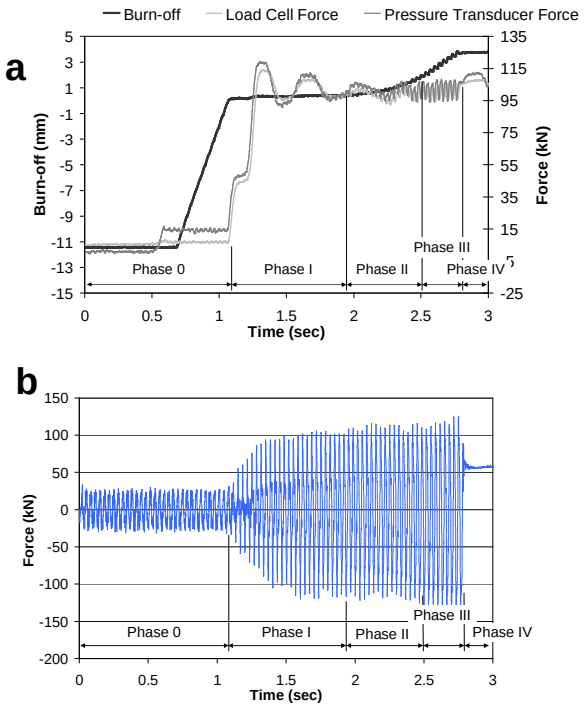

Fig. 3 Machine data generated during the linear friction weld performed at a frequency of 30 Hz and a rubbing velocity of 549 mm s^{-1}. (a) Burn-off, and axial load measured with a load cell and pressure transducer; (b) in-plane force, F_l.

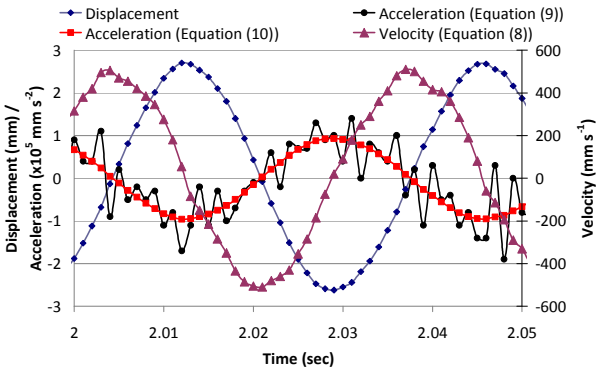

Fig. 4 Plot of displacement, velocity and acceleration versus time for a frequency of 25 Hz and rubbing velocity of 470 mm s^{-1}.

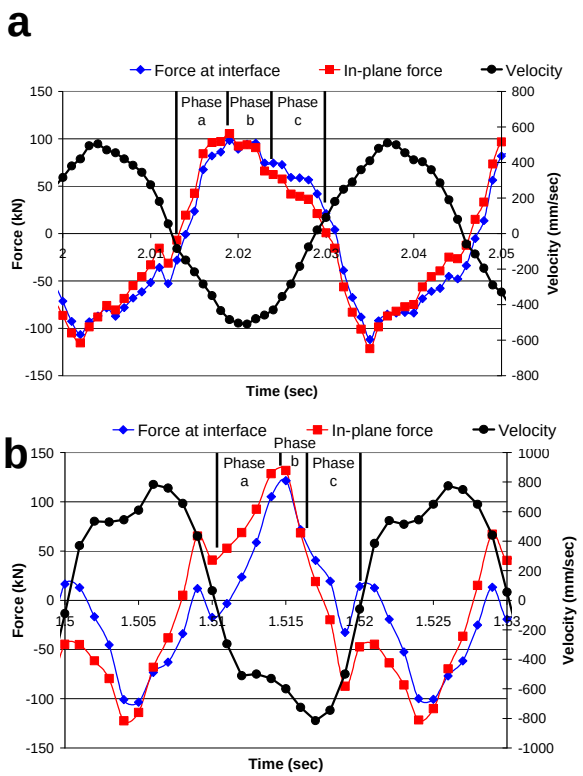

Fig. 5 Plots of in-plane and interface forces and rubbing velocity versus time for (a) 25 Hz, 470±1 mm s^{-1}, (b) 50Hz, 863±1 mm s^{-1}. The velocity is inverted for clarity.

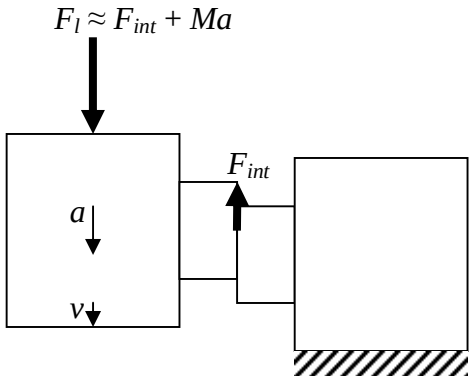

Phase a – Acceleration phase

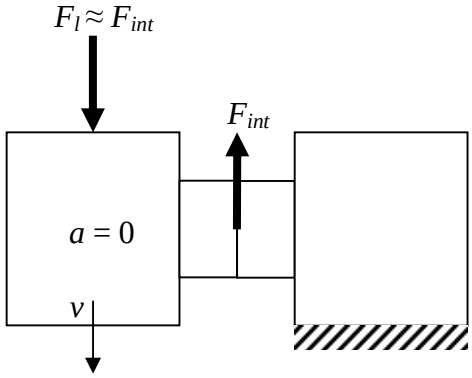

Phase b – Constant velocity phase

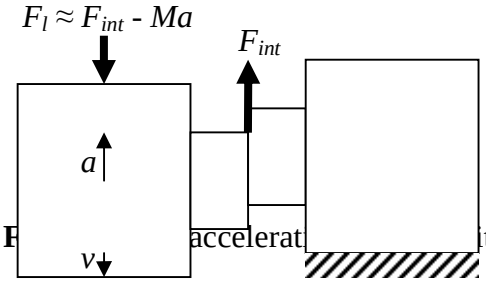

F acceleration during one stroke of LFW.

Phase c – Deceleration phase

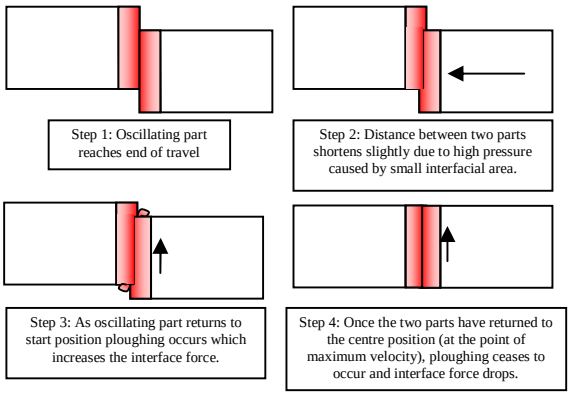

Fig. 7 Suggested ploughing mechanism which occurs during LFW

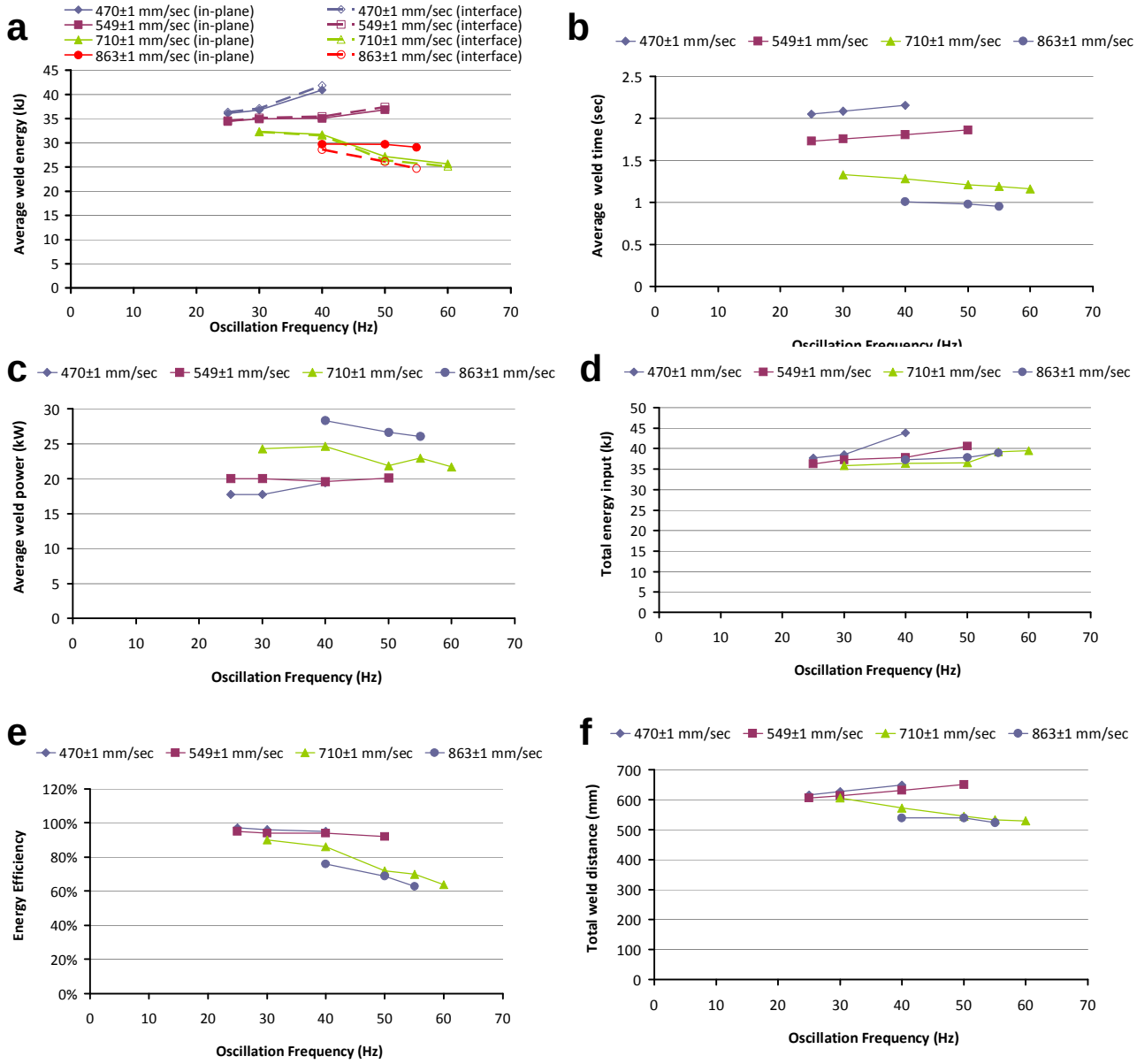

Fig. 8 (a) In-plane and interface energy input during welding only (phases I, II and III); (b) average duration of the weld (phases I, II and III); (c) average weld power (phases I, II and III); (d) total energy input (including phase 0, based on in-plane force); (e) energy efficiency calculated by dividing the weld energy (based on interface energy for phases I, II and III) by the total in-plane energy input (phases 0, I, II and III) and (f) total weld distance.